



GEOSCIENCES

Comparing explosive cyclogenesis cases of different intensities occurred in Southern Atlantic

VILSON D. DE AVILA, ANDRÉ B. NUNES & RITA DE CÁSSIA M. ALVES

Abstract: Six events of explosive cyclogenesis occurred in the south Atlantic were compared using reanalysis data and satellite water vapor imagery. Cases of different intensities (weak, moderate and strong) occurred during 2014 summer season and 2012 winter season were studied. Despite the similarities the tropopause anomaly was more prominent and vertical movements were stronger in the strong cyclogenesis cases. The tropopause anomalies behind the cold front and ahead of the warm front appear only in the mature stage of the weak and moderate cases while in the strong case it is already evident and more intense behind the cold front since the beginning of the cycle. In all the cases confluence of the jet streams took place at higher levels forming a jet streak with diffluence occurring downstream and the cyclone beginning in the exit region. The trajectories of the cyclones were in the southeast direction but longer and more meridional in the strong cases. The results indicated the baroclinicity of the region as the main mechanism for the development of these cyclones as well as the amplitude of the upper level jet stream perturbation. Furthermore, all the explosive cyclones developed following the Shapiro & Keyser cyclone conceptual model.

Key words: explosive cyclone, tropopause anomaly, Shapiro-Keyser, seclusion.

INTRODUCTION

The southern region of South America is very influenced by the passage of many types of meteorological transient systems such as fronts, cyclones, squall lines, mesoscale convective systems and even tornados.

Generally, in the absence of climatic anomalies the south region of Brazil, Paraguay and Uruguay have a practically homogeneous precipitation regime with territorially well distributed precipitations along the year with elevated annual totals (Reboita et al. 2010) which favors the agricultural activities, the vegetable extractivism, the livestock farming and the hydroelectric energy production as in

the case of the Itaipu Dam, one of the world's biggest hydroelectric power plants.

The weather and climate of the southern region of South America are strongly influenced by the occurrence of extratropical cyclones since this kind of meteorological transient system and their associated fronts are the most frequent phenomena reaching the region (Reboita et al. 2010) and maintaining the regime of abundant and well distributed precipitation in space and time.

The first cyclone conceptual model was designed by Bjerknes (1919), improved by Bjerknes & Solberg (1922), followed by works like Sutcliffe (1947), Petterssen (1956), Palmen & Newton (1969), among many others, with the

publication of an additional conceptual model proposed by Shapiro & Keyser (1990).

Till 1990 there were a few studies about cyclogenesis in South America (e.g., Taljaard 1967, Necco 1982, Satyamurty et al. 1990). They found discrepant results because of the different periods in time and size as well as the data used. In order to understand the actual behavior of cyclogenesis Gan & Rao (1991) computed the frequency of surface cyclogenesis over South America during the period of 1979-1988. From the 1091 cases observed in that period they found that the frequency of cyclogenesis is higher in the winter in accord to Necco (1982) with the maximum frequency in May and the minimum in December. In addition to the seasonal variation of cyclogenesis they find interannual variation with major frequency in El Niño years and also spatial variation with emphasis to two preferred regions for the occurrence of cyclogenesis: One in the region of Uruguay where the major frequency was in the winter influenced by the Andes Cordillera and the baroclinic instability, and the other near the San Mathias gulf where the frequency was higher in the summer associated to the baroclinic instability of the westerly flow.

After 1990 automatic schemes for detection and tracking of cyclones and anticyclones were developed (Murray & Simmonds 1991) and many works utilized reanalysis data with different spatial and temporal resolutions (Sinclair 1995, Mendes et al. 2010). As an example, Sinclair (1995) utilized reanalysis data from European Centre for Medium-Range Weather Forecasts (ECMWF) while Simmonds & Keay (2000) utilized reanalysis data from National Centers for Environmental Prediction / National Center for Atmospheric Research (NCEP/NCAR) and both obtained results that agreed and confirmed those results obtained by Gan & Rao (1991).

Thereafter, other studies found the existence of more cyclogenetic regions in South America. Hoskins & Hodges (2005) and also Reboita et al. (2005) found a third cyclogenetic region in the east coast to the south and southeast of Brazil with higher frequency of events in the summer. Allen et al. (2010) found another cyclogenetic region in the south extreme of South America.

Among the extratropical cyclones there is a special kind which develops in a very rapid and intense way with respect to the deepening of the central atmospheric surface pressure. This kind of cyclone is frequently referred as Bomb Cyclone (Bluestein 1993), commonly Explosive Cyclone and also East Coast Cyclone. They generate severe weather causing serious risk in regions near the coast because they are potentially destructive and difficult to predict due to the very fast deepening of the central surface pressure, to the lack of meteorological observation data over the ocean as well as knowledge of the dynamic and thermodynamic factors that determine their occurrence.

Originally the explosive cyclogenesis is characterized by an intense and rapid deepening in the surface pressure originally defined as a pressure drop of at least 1 hPa/h during a 24 hours period in the latitude of 60°. The criterion for its recognition corrected for any latitude is the value of the Normalized Deepening Rate (NDR) of the central surface pressure (Sanders & Gyakum 1980) given in Bergeron units (B) as:

$$NDR = \left[\Delta p \left(\frac{\sin \phi}{\sin 60^\circ} \right) \right] / 24 \text{ hours} \quad (1)$$

In this equation ϕ is the mean latitude of the explosive cycle and is the surface pressure drop during that cycle. When the NDR reaches at least 1 B the cyclogenesis is considered explosive.

According to Sanders & Gyakum (1980) the explosive cyclones produce great amounts of precipitation, strong winds, high waves, and poor

visibility. They are included among the most severe events that affect the coastal regions where the demographic density is high and also in the open sea.

Various authors (e.g., Hoskins et al. 1985, Uccellini et al. 1985, Wang & Rogers 2001, Avila et al. 2016, Nunes & Avila 2017) have indicated the association between the variations in the tropopause height and the occurrence of surface cyclogenesis. It was observed that the occurrence of tropopause local lowering frequently referred as “tropopause folding” (Reed 1955) was remarkable in cases of explosive cyclogenesis. In some articles as Santurette & Georgiev (2005) it was shown that the surface of 1.5 Potential Vorticity Unit (PVU) is representative of the so called “dynamic tropopause” although some authors consider 1.0 PVU and others even 2.0 PVU. Bechis et al. (2018) suggested that the Ertel Potential Vorticity (EPV) threshold corresponding to the dynamic tropopause (indicated by the World Meteorological Organization as -1.6 PVU for Southern Hemisphere) should take into account the seasonality and the topography for its determination. Thus it is common in Meteorology to identify the tropopause height by the Ertel Potential Vorticity (Hoskins et al. 1985, Schubert et al. 2004) with value of 1.5 PVU (where $1 \text{ PVU} = 1 \times 10^{-6} \text{ K kg}^{-1} \text{ m}^2 \text{ s}^{-1}$, having positive sign in the Northern Hemisphere and minus sign in the Southern Hemisphere).

The satellite water vapor imagery is useful for identifying the dry air intrusions associated with the tropopause folding as dark narrow bands (Santurette & Georgiev 2005).

The surface sensible and latent heat fluxes have been appointed by some authors (e.g. Piva et al. 2011, Pezzi et al. 2016) as important in the cyclogenetic processes. Giordani & Caniaux (2001) have also emphasized the role of sensible and latent heat fluxes in explosive cyclogenesis.

Pinto & Rocha (2011) used the Lorenz Energy Cycle to analyze the cyclogenesis dynamic aspects over the east coast cyclogenetic region of South America founding that the cyclogenesis may have various different features there. In a pioneering way Black & Pezza (2013) have analyzed the Lorenz Energy Cycle associated with explosive cyclogenesis for the four regions with major explosive activity of the globe and found a robust signature in that energy cycle associated to anomalous energy conversion that are not present in normal cyclogenesis processes. The latter believe that their results open a new way to explore the behavior of explosive storms based on the great scale environment and may provide its prediction.

Various studies on explosive cyclogenesis were made for South America focusing mainly climatological aspects (e.g., Mendes et al. 2010, Bittencourt et al. 2013), the role of surface sensible and latent heat fluxes (Piva et al. 2011) and some others concerning certain dynamic or synoptic features (e.g., Iwabe & Rocha 2009, Avila et al. 2016).

Bittencourt et al. (2013) presented a climatologic study for the explosive cyclones in the South America cyclogenetic region based on NCEP reanalysis data and tracking automatic scheme of Murray & Simmonds (1991). They found that explosive cyclones are more frequent in the winter being a rare phenomenon although the South America cyclogenetic area has the major frequency of such cyclones in the southern hemisphere. Their results agree with those of Lim & Simmonds (2002).

The above exposed leads to the motivation of the present work aiming improvement of the knowledge about the explosive cyclones in order to contribute for their prediction and consequent mitigation of losses caused by them.

The specific objectives consist of comparing some cases of explosive cyclogenesis with

different intensities occurred in the seasons of summer and winter with respect to the central surface pressure deepening rate and the behavior of the Dynamic Tropopause Anomaly coupled with other meteorological variable fields.

MATERIALS AND METHODS

To obtain the meteorological fields that allows observing the relation between the variables which describe the life cycle of the explosive cyclones with tropopause foldings, we made use of reanalysis datasets of The Modern Era Retrospective-Analysis for Research and Applications (MERRA), developed at Goddard Space Flight Center of National Aeronautics and Space Administration (GSFC/NASA) in its MERRA-2 version (Gelaro et al. 2017), with a longitude resolution of 0.66° and a latitude resolution of 0.5° . The temporal domain was the period comprehended between 2012 and 2016 and the interval was six hours. The spatial domain was limited by latitudes of 0° - 70° S and longitudes of 90° W- 0° .

The MERRA-2 reanalysis datasets were used in several studies such as Quadro et al. (2012), Avila et al. (2016), being compared with other reanalysis datasets (e.g. Hodges et al. 2011), and also compared with satellite data (e.g. Naud et al. 2014).

The following MERRA-2 variables were used here: Mean Sea Level Pressure (MSLP), geopotential height (H), horizontal wind speed components (u and v), vertical velocity in isobaric coordinate system (ω), air temperature (T), surface sensible and latent heat fluxes, Ertel potential vorticity (EPV) and relative humidity (rh). These data were visualized by the GRADS® software.

We also used satellite imagery from the Geostationary Operational Environmental

Satellite – 13 (GOES-13) in the channel 3 of water vapor obtained from Satellite Division and Environmental Systems of National Institute for Space Research (Divisão de Satélites e Sistemas Ambientais do Instituto Nacional de Pesquisas Espaciais - DSA/INPE).

First the explosive cyclones were detected by the direct visual inspection of the sea level pressure analysis made with GrADS®, and the Equation 1;

After detection the cases were classified by intensity second the Sanders (1986) criterion as follows:

- $1.0 B \leq \text{Weak} < 1.3 B$;
- $1.3B \leq \text{Moderate} < 1.8 B$ and
- $\text{Strong} \geq 1.8 B$

Then, for the present work three cases of explosive cyclogenesis with different intensities were selected both for 2014 summer season and 2012 winter season and compared by:

The EPV field as an identifier of the Dynamic Tropopause and its anomalies;

Analysis of EPV coupled with other fields to find their behavior in the presence of tropopause folding;

Dry stratospheric air intrusions recognizing by the satellite water vapor imagery;

Analyze the 250 hPa and 850 hPa stream lines to observe the upper level jet streams perturbations and the flow at lower levels respectively.

RESULTS AND DISCUSSION

Following the methodology, an expressive number of 152 cases were found in a period of only five years. This number is higher than the 144 cases found by Bitencourt et al. (2013) in a much longer period of 54 years. It must be emphasized the contribution of the direct inspection of the MSLP field as well as the wider domain and

the better quality of the higher resolution data for the results in the present work. Despite the differences some aspects agreed in both procedures, e.g. the higher number of cases in the winter season and a mean of two strong cases per year. The cases found here and their intensities can be seen in Figure 1 which shows a high monthly variability in the frequency of explosive cyclogenesis occurrence independent of intensity with maximum occurrence in August followed by July. In general the number of cases had an inverse relationship with intensity except in the spring when the moderate cases exceeded

the weak cases. It is noticeable the lacking of strong cases in 2016 despite the occurrence of most of the cases in that year and various moderate cases almost reached classification as strong explosive cyclogenesis suggesting the absence of strong cases as a consequence of the rigor in the choice of the intensity thresholds.

From those cases found it was selected one case of each of the three intensities for the summer and the winter seasons. The choice of the cases took into account the following criteria: 1) Belonging to the opposed seasons proposed; 2) Occurred in neutral ENSO (El Niño

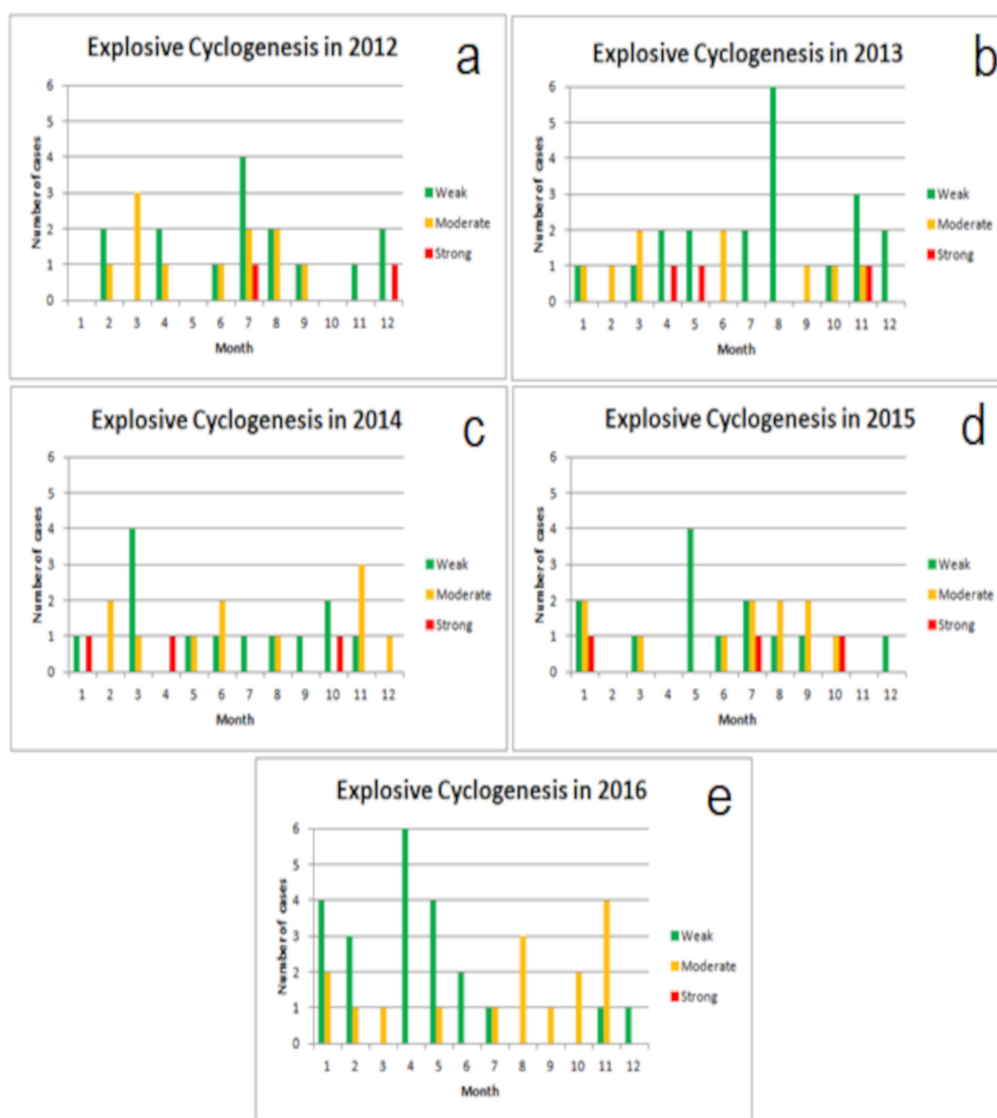


Figure 1. Distribution of the explosive cyclogenesis cases second the intensity for the 2012-2016 period: a) 2012, b) 2013, c) 2014, d) 2015, e) 2016.

– Southern Oscillation) periods and 3) Covering the three referred intensities. For convenience aiming the proposed objective the order adopted was the season (summer and winter) and intensity (strong, moderate and weak) instead of chronological order. Thus, one case of each of the three intensities was selected for the 2014 summer and the 2012 winter.

Figure 2 shows the selected summer cases of 2014. The initial positions of the explosive development can be seen by the MSLP fields in Figure 2 (a, c, e) while the final position, as well

as the trajectories showing the positions at six hours intervals can be seen in the Figure 2 (b, d, f).

Figure 2a shows the cyclone beginning its explosive development in 01/03/2014 at 00Z with a central surface pressure of 996 hPa located at 40°S, 47°W which presented a pressure drop of 42 hPa in 24 hours while moving southeast until 01/04/2014 at 00Z when reached 52°S, 35°W with a central pressure of 954 hPa (Figure 2b). The computed NDR for this mean latitude of 46° and this pressure drop was 2.1 B classifying

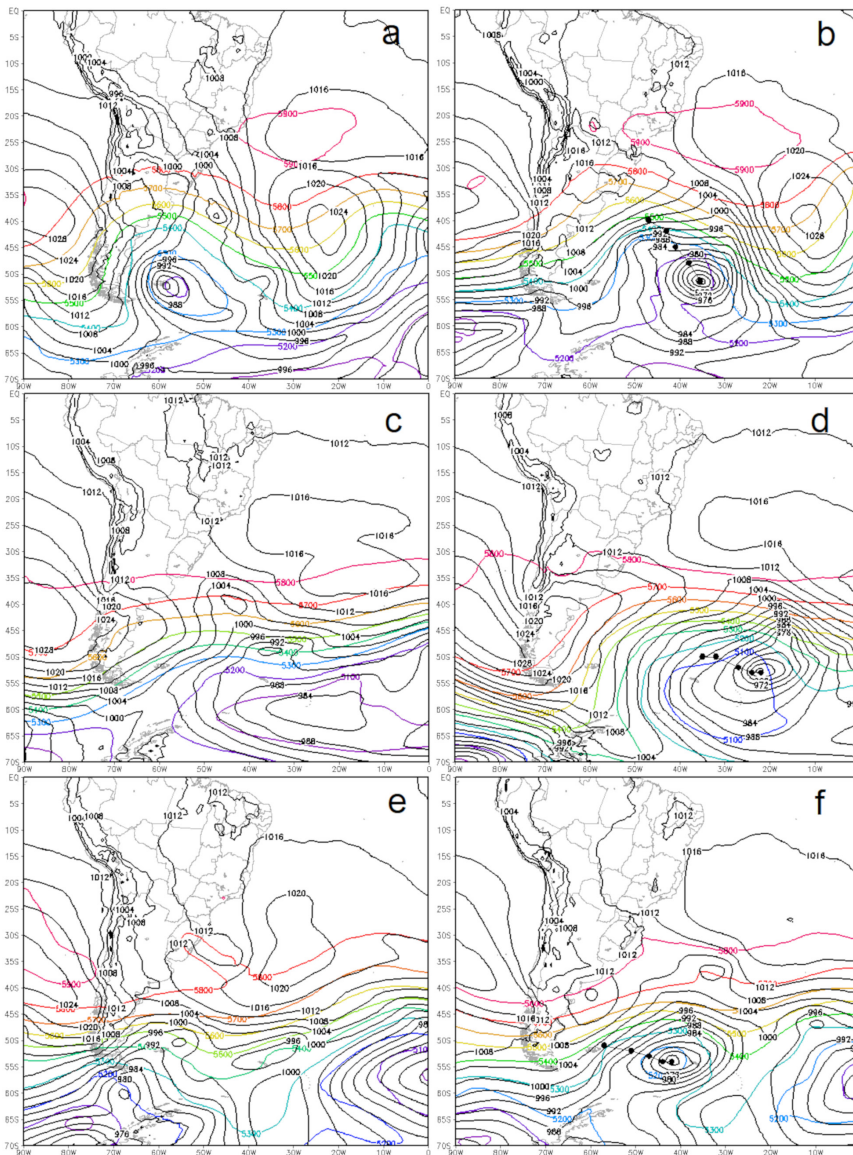


Figure 2. MSLP (black contours) and 500 hPa geopotential height (color contours) at the beginning of the explosive cycle of the cyclones (a- 01/03/ 2014, 00Z; c- 02/12/2014, 12Z; e- 01/15/2014, 00Z), and at the end of the explosive cycles with 6-6 hours trajectories (b- 01/04/2014, 00Z; d- 02/13/2014, 12Z; f- 01/16/2014, 00Z)¹.

Footnote 1, related to Figure 2:

¹Dates are on the north American month/day/year format.

this case as strong explosive cyclogenesis. This case presented an additional pressure drop of 8 hPa during the next 12 hours after the explosive development.

Figure 2c shows the cyclone beginning its explosive development in 02/12/2014 at 12Z with a central surface pressure of 988 hPa located at 50°S, 37°W which presented a pressure drop of 30 hPa in 24 hours while moving southeast until 12Z of 02/13/2014 when reached 53°S, 21°W with a central pressure of 958 hPa (Figure 2d). The computed NDR for this mean latitude of 52° and this pressure drop was 1.37 B classifying this case as moderate explosive cyclogenesis.

Figure 2e shows the cyclone beginning its explosive development in 01/15/2014 at 00Z with a central surface pressure of 992 hPa located at 51°S, 56°W which presented a pressure drop of 24 hPa in 24 hours while moving southeast until 01/16/2014 at 00Z when reached 55°S, 42°W with a central pressure of 968 hPa (Figure 2f). The computed NDR for this mean latitude of 53° and this pressure drop was 1.08 B classifying this case as weak explosive cyclogenesis.

It's noticeable in Figure 2 that the strong case began in much lower latitude and its trajectory was much longer having an enhanced meridional component while the moderate and weak cases initiated at higher latitudes with trajectories almost zonal. The weak case initiated near the continent and the moderate farther from the coast.

Comparing these three cases in the beginning of the explosive cycles (Figure 2a, 2c, 2e) with respect to the geopotential height of the 500 hPa level, it becomes evident the lagging of the 500 hPa trough to the west relative to the surface low pressure center, that is an inclination of the vertical trough axis to west indicating the baroclinicity of the systems. The vertical trough axis had a much smaller inclination in the weak case. The 500 hPa geopotential contours

suggests a larger amplitude perturbation of the upper level flow in the strong case, being smaller in the moderate case and even smaller in the weak case.

Figure 2 (b, d, f) shows the final of the explosive development of the cyclones when the 500 hPa troughs were in phase with the surface low pressure centers indicating the barotropic state of the mature stage of the cyclones. In this stage the vertical trough axes had no more the initial inclinations to the west and in the strong case even inverted the inclination to the east during the twelve hours of subsequent surface pressure deepening.

Figure 3 shows the selected cases of explosive cyclogenesis occurred in the winter of 2012 in the MSLP field coupled with geopotential height of the 500 hPa pressure level.

Figure 3a shows the cyclone beginning its explosive development in 07/30/2012 at 06Z with a central surface pressure of 992 hPa located at 40°S, 35°W which presented a pressure drop of 44 hPa in 24 hours while moving southeast until 07/31/2012 at 06Z when reached 56°S, 19°W with a central pressure of 948 hPa (Figure 3b). The computed NDR for this mean latitude of 48° and this pressure drop was 2.13 B classifying this case as strong explosive cyclogenesis.

Figure 3c shows the cyclone beginning its explosive development in 07/13/2012 at 00Z with a central surface pressure of 1000 hPa located at 33°S, 43°W which presented a pressure drop of 24 hPa in 24 hours while moving southeast until 07/14/2012 at 00Z when reached 44°S, 34°W with a central pressure of 976 hPa (Figure 3d). The computed NDR for this mean latitude of 38.5° and this pressure drop was 1.39 B classifying this case as moderate explosive cyclogenesis.

Figure 3e shows the cyclone beginning its explosive development in 07/10/2012 at 12Z with a central surface pressure of 1004 hPa located at 42°S, 47°W which presented a pressure drop

of 24 hPa in 24 hours while moving southeast until 07/11/2012 at 12Z when reached 53°S, 40°W with a central pressure of 980 hPa (Figure 3f). The computed NDR for this mean latitude of 47° and this pressure drop was 1.18 B classifying this case as weak explosive cyclogenesis.

All the three winter cases showed in Figure 3 initiated at lower latitudes and had long trajectories with enhanced meridional components. In all the winter cases the lagging of the 500 hPa trough relative to the surface low pressure center was also observed in the beginning of the explosive cycle as well as the

barotropic stage in the final when the vertical trough axes became vertically aligned. Despite the weak case presented more inclination of the vertical trough axis in the beginning, it actually had the same pressure drop of the moderate case which resulted in a smaller NDR due to its higher mean latitude.

Figure 4 shows the vertical sections of $EPV \geq 1,5UPV$ in module (remembering that the EPV is negative in the southern hemisphere) taken in the initial and final latitudes of the explosive cycle of the summer cases. The strong case (Figure 4a, 4d) exhibited a

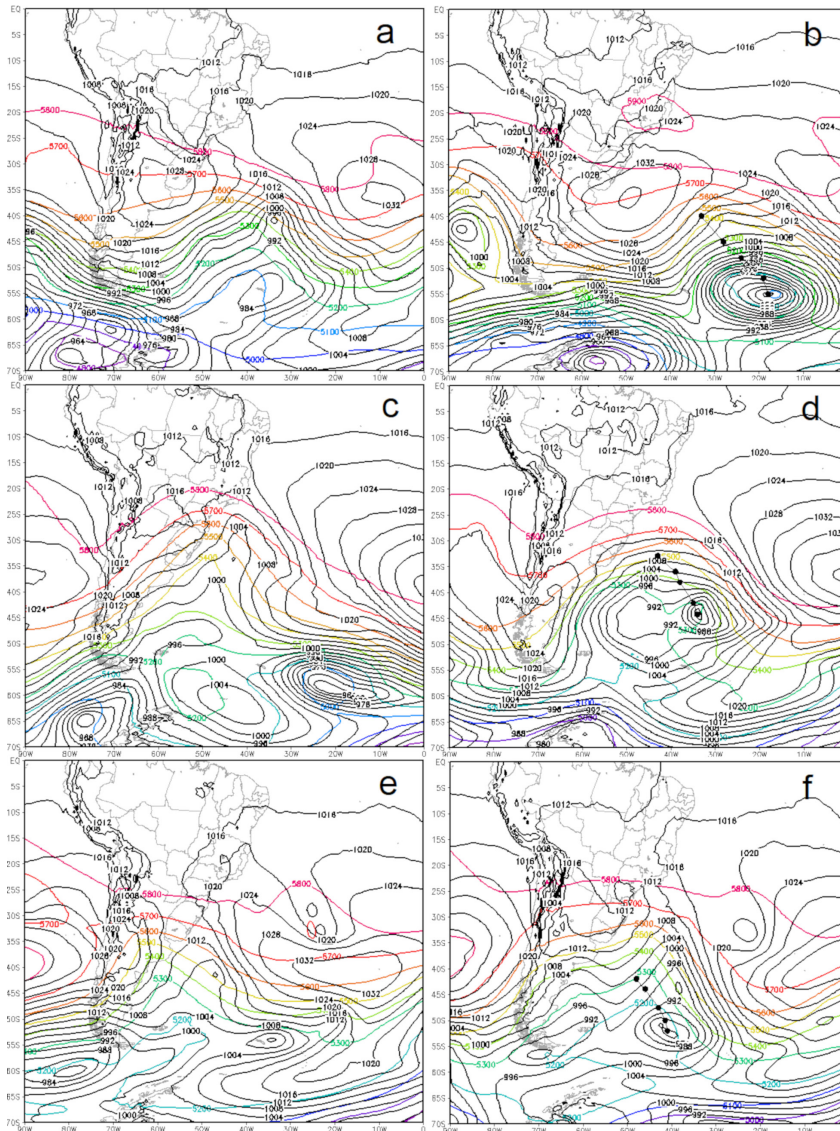


Figure 3. MSLP (black contours) and 500 hPa geopotential height (color contours) at the beginning of the explosive cycle of the cyclones (a- 07/30//2012, 06Z; c- 07/13/2012, 00Z; e- 07/10/2012, 12Z), and at the end of the explosive cycles with 6-6 hours trajectories (b- 07/31//2012, 06Z; d- 07/14/2012, 00Z; f- 07/11/2012, 12Z).

Dynamic Tropopause Anomaly (DTA) much more prominent than the moderate (Figure 4b, 4e) and weak cases (Figure 4c, 4f). Otherwise the moderate and weak cases presented a wider response in the surface probably because of the lower tropopause height in the higher latitudes where they initiated.

Figure 5 is analog of Figure 4 for the winter cases. Figure 5a and 5d show the EPV in the beginning and in the end of the strong case explosive cycle, respectively. It may be seen that the DTA was much more vigorous in the strong case than in the moderate (Figure 5b, 5e) and in the weak cases (Figure 5c, 5f).

From Figure 6 to Figure 11 the satellite imagery of water vapor is shown for each case at the beginning (a and c) and at the end (b and d) of

the explosive development accompanied by the corresponding 500 hPa EPV coupled with MSLP.

Figure 6 shows the strong summer case. The satellite water vapor image (Figure 6a and 6b) exhibited an enhanced dark band oriented southeast ending in the center of the cyclone which is indicative of the dry air intrusion from the lower stratosphere into the high and mid troposphere through the tropopause folding. In Figure 6c and 6d it can be readily seen the band with high values in the 500 hPa EPV identifying the DTA coinciding with that tropopause folding detected by the satellite. The referred band was located behind the cold front and rotated tending to turn parallel to that.

Figure 7 shows the moderate summer case. As in the strong case the satellite images

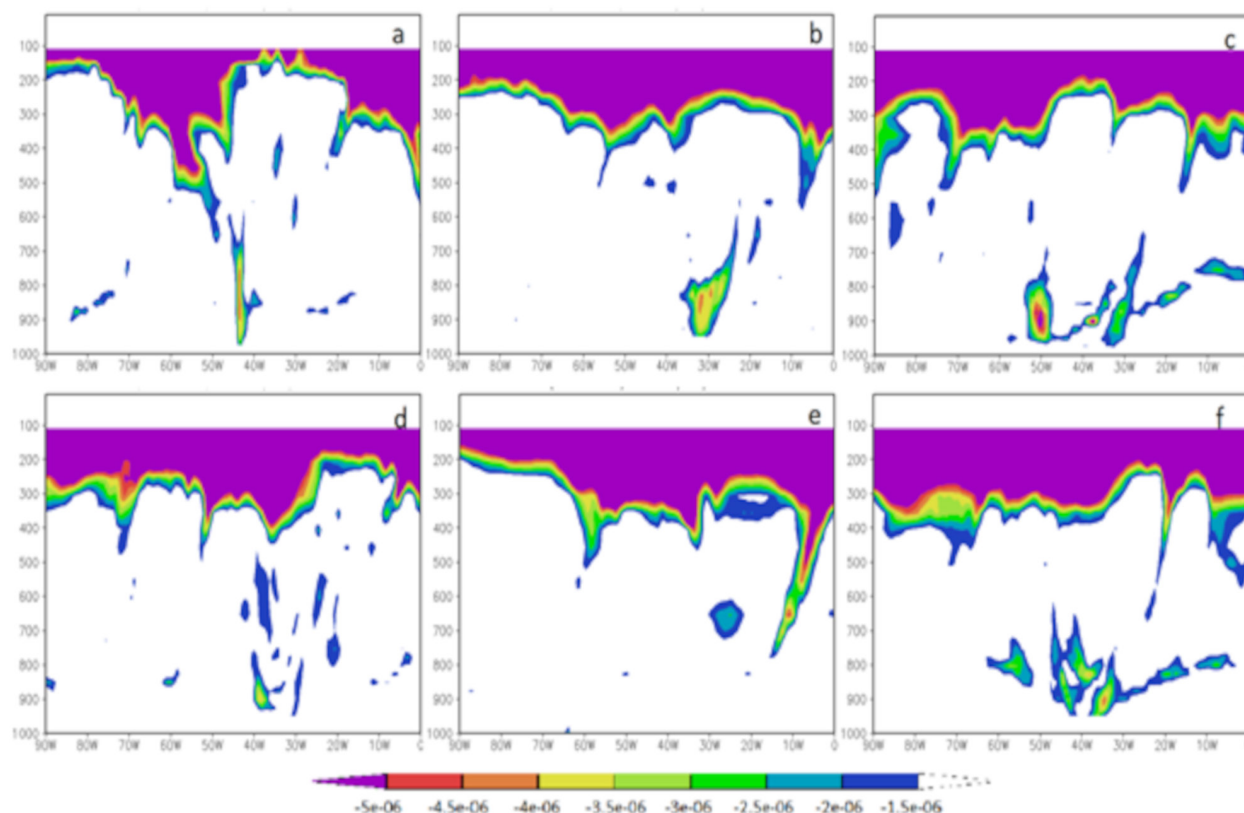


Figure 4. Vertical zonal sections of EPV \geq 1,5PVU (in module) with color shading in the latitudes where the cyclones were localized at the beginning of the explosive development: (a- 01/03/2014, 00Z, 40°S; b- 02/12/2014, 12Z, 50°S; c- 01/15/2014, 00Z, 51°S), and at the end of the explosive cycle: (d- 01/04/2014, 00Z, 50°S; e- 02/13/2014, 12Z, 53°S; f- 01/16/2014, 00Z, 55°S).

(Figure 7a and 7b) exhibited large dark regions corresponding to dry air of the anticyclones and narrow dark bands corresponding to stratospheric dry air intrusion into the troposphere through the tropopause folding. Figure 7a shows the narrow band of dry air intrusion in the region of the incipient cyclone center with a slight southeast orientation becoming almost zonal in the end (Figure 7b). The 500 hPa EPV had not evidenced the ATD in the beginning (Figure 7c) because the tropopause folding had not reached the 500 hPa level while in the end (Figure 7d) the ATD was evident behind the cold front and also behind the warm front.

Figure 8 shows the weak summer case. In the satellite imagery (Figure 8a and 8b) a narrow dark band which was associated with

another cyclone can be seen extending from Uruguay towards southeast. The weak case cyclone initiated over Malvinas Islands and the associated tropopause folding extended from south of Pacific Ocean crossing the south extreme of South America till it reaches the region over the incipient cyclone. The ATD was apparent since the beginning in the 500 hPa EPV (Figure 8c). The orientation of the band was almost zonal being slightly counterclockwise in the Pacific Ocean and clockwise after crossing the extreme of the continent. Furthermore the humidity gradient was quite weak.

Figure 9 shows the strong winter case. The water vapor satellite imagery (Figure 9a and 9b) exhibited a well defined dry band also evidenced in the 500 hPa EPV (Figure 9c and 9d) indicating

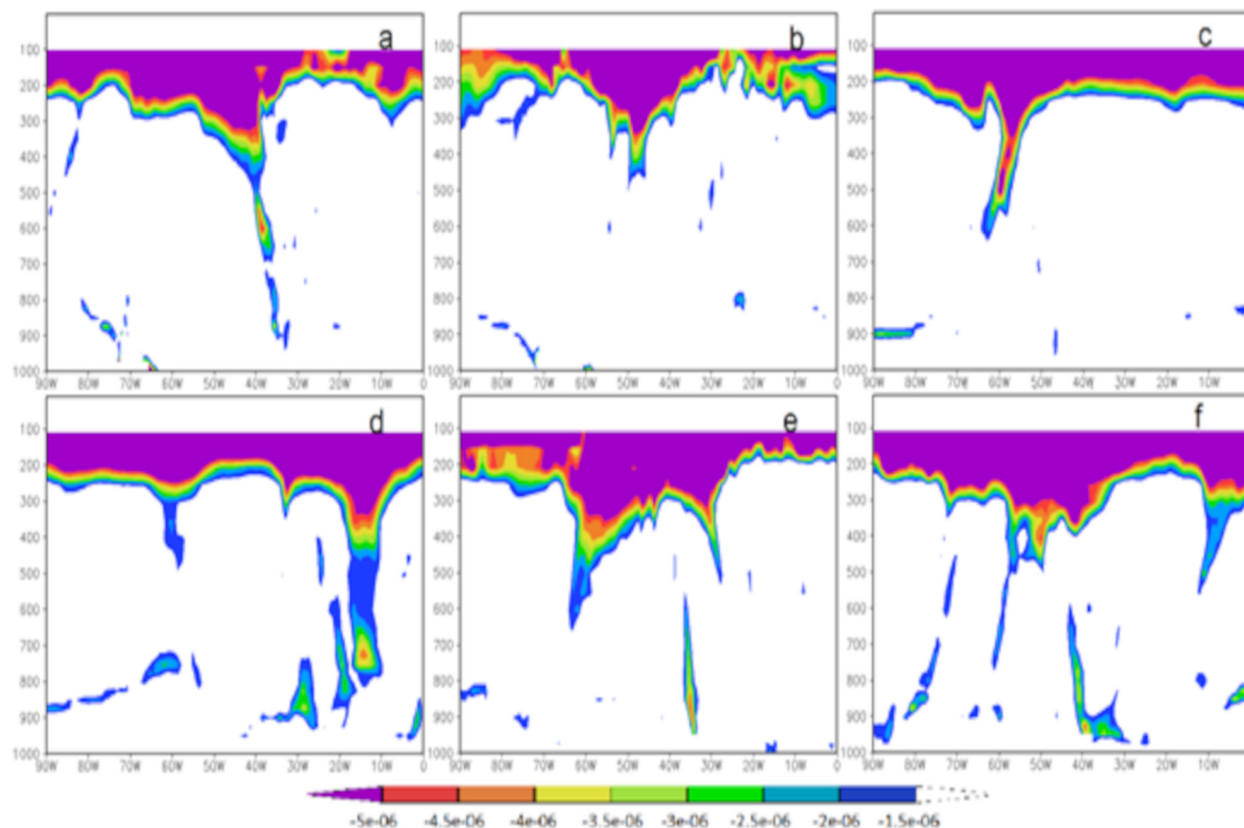


Figure 5. Vertical zonal sections of $EPV \geq 1,5$ PVU (in module) with color shading in the latitudes where the cyclones were localized at the beginning of the explosive development: (a- 07/30/2012, 06Z, 40°S; b- 07/13/2012, 00Z, 33°S; c- 07/10/2012, 12Z, 42°S), and at the end of the explosive cycle: (d- 07/31/2012, 06Z, 56°S; e- 07/14/2012, 00Z, 44°S; f- 07/11/2012, 12Z, 53°S).

the intrusion of dry stratospheric air with high values of EPV into the troposphere. As in the other cases a “cloud head” was observed in the occluded region.

Figure 10 shows the moderate winter case. The water vapor imagery (Figure 10a and 10b) showed a sharp humidity gradient defining the tropopause folding. However in the 500 hPa EPV (Figure 10c and 10d) the ATD was not evident mainly because of the higher tropopause height of these lower latitudes. In this case the satellite imagery showed clearly that the cyclone developed following the Shapiro & Keiser (1990) conceptual cyclone model. It can be also observed in the other cases despite some limitations caused by the smaller satellite spatial domain.

Figure 11 shows the weak winter case. The tropopause folding evolved in an unusual way. There was a more evident tropopause folding which passed by Bahia Blanca, Argentina (Figure 11a and 11c) associated with an older cyclone in the south, and a secondary tropopause folding (not apparent in the 500 hPa EPV field in Figure 11c) passing through Uruguay and reaching the explosive cyclone region. In the end of the cycle the tropopause folding had an abrupt change in direction becoming almost meridional in the cyclone region while the evolution following the Shapiro & Keiser conceptual model became evident.

Figure 12 and 13 shows the 250 hPa stream lines of the summer and winter cases respectively. In both figures parts a, b and c

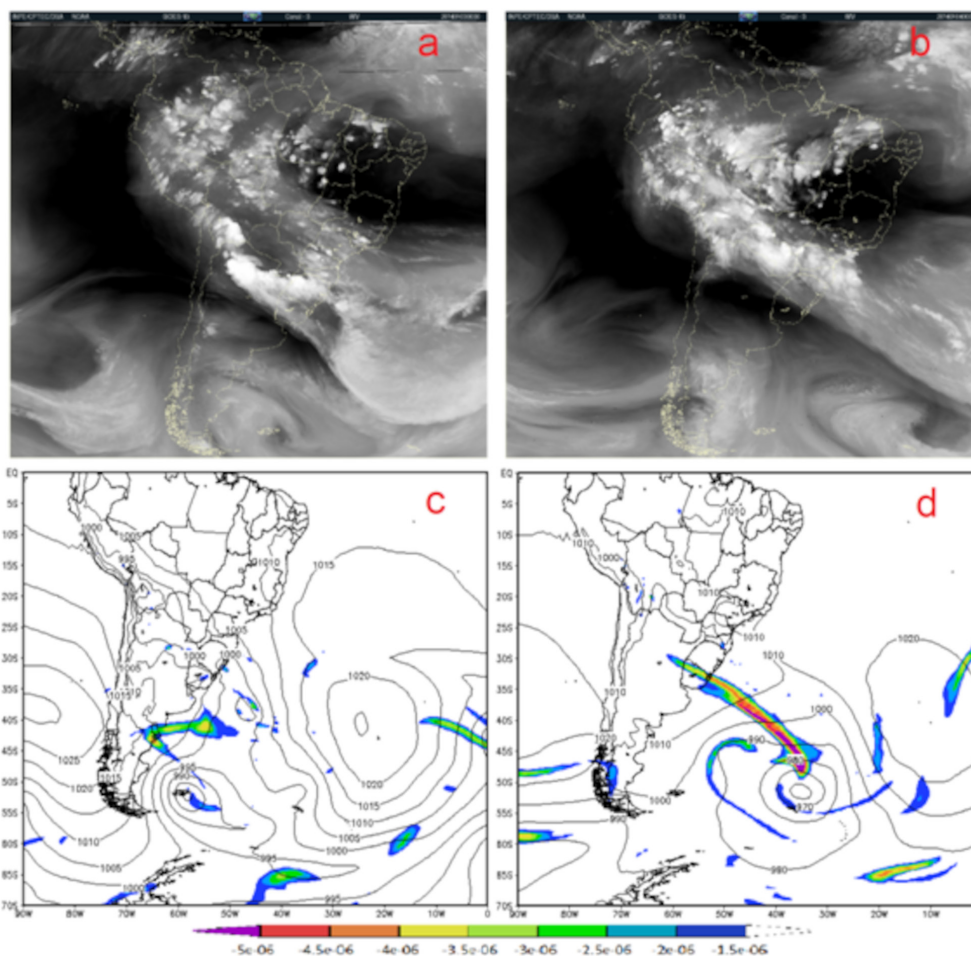


Figure 6. Satellite GOES-13 water vapor channel imagery (above) and EPV in the 500 hPa level (color shaded) with MSLP contours (below) respectively in the beginning of the explosive development of the cyclone (a and c – 01/03/2014, 00Z) and at the end of this cycle (b and d – 01/04/2014, 00Z).

corresponds to the beginning of the strong, moderate and weak cases respectively, while parts d, e and f corresponds to the end of the explosive development in the same order. Figure 12a and 12d shows the strong summer case with a jet stream more perturbed and intense than the other cases.

In the winter cases (Figure 13) the jet streams are not so intense despite being quite perturbed.

In all cases studied here it was possible to observe the confluence of the subtropical and polar jet streams over the continent under the influence of the upper level circulation which is anticyclonic on the equatorial side of the subtropical jet stream and cyclonic on the polar side of the polar jet stream. In the confluence of the jet streams occurs a jet streak (i.e. a maximum speed in the jet stream) with diffluence occurring downstream near the east coast or in the Atlantic Ocean. The explosive cyclogenesis in the surface takes place below the exit region of the jet streaks (Note: the figures shown here represents only the explosive cycles, but the whole life cycle of the cyclones and the analyses which led to the above considerations were not limited to the referred explosive cycle).

In the 850 hPa stream lines (not showed here) it was observed in the strong summer case the flow conducting warm humid air from the Amazonian Forest to the region where the cyclone developed during the whole life cycle. In the summer moderate case it was observed that the contribution from the Amazon Forest with warm humid air occurred only during the first half of the explosive cycle. In the weak summer case there was not any contribution from the Amazonian flow for the explosive cyclogenesis.

Also in the strong winter case as well as in the moderate winter case there was not any contribution from the Amazonian flow for the explosive cyclogenesis, while in the weak winter

case it was observed some contribution only in the beginning of the explosive development.

Figures 14 (summer cases) and 15 (winter cases) show vertical zonal sections with contours of $EPV \geq 1,5PVU$ (in module) and color shaded vertical velocity in isobaric coordinate system (ω). All cases presented subsident movements predominating west of the ATD and ascendant movements east of the ATD in the beginning and during part of the explosive development while in the final ascendant movements predominated.

Figures 16 (summer cases) and 17 (winter cases) show vertical zonal sections with contours of $EPV \geq 1,5PVU$ (in module) and color shaded relative humidity (%). In that figures all the strong cases (a, d), moderate cases (b, e) and weak cases (c, f) showed relative humidity values between 10 and 20% coinciding with the dynamic tropopause and also with the regions of downward movement. Values higher than 60% can be seen mainly in lower levels and in regions of upward movement.

Figures 18 and 19 show the latent heat fluxes for the summer and winter cases respectively.

In the beginning of the summer cases the latent heat fluxes appear behind the cold front reaching values of $450 W/m^2$ in the final of the strong case (Figure 18a and 18d) and $400 W/m^2$ in the moderate case (Figure 18b and 18e) while in the weak case (Figure 18c and 18f) it does not exceed $300 W/m^2$.

In the beginning of the winter cases (Figure 19) the latent heat fluxes appear behind the cold front reaching values of $300 W/m^2$. Such values were lower than that of the summer season mainly because the water surface is colder in that winter season.

The sensible heat fluxes due to turbulence were negligible in the beginning of all the summer cyclogenesis cases presented here (Figure 20) reaching significant positive values in

the end of the explosive cycles behind the cold front and negative values of smaller magnitude behind the warm front. In the winter cases (Figure 21) the positive values of sensible heat fluxes due to turbulence behind the cold front were smaller reaching about 100 w/m^2 while the negative values behind the warm front occupied a wider area in the moderate and weak cases.

In conclusion, it should be highlighted that this work did not aim at a synoptic climatology of explosive cyclones. Here, a detailed interpretation of the large-scale environment was made regarding six cases of explosive cyclones of different intensities. The analysis by composite fields was not performed here since the events took place in different locations in the South Atlantic. Therefore, the synoptic configuration of the cases does not necessarily represent the average behavior of the phenomenon. Even so, the features found here will serve as a reference for future works on cyclone bombs, specially in the South Atlantic.

From the analysis of the six cases presented here we concluded that despite the differences in various aspects like intensity and seasonality as well as initial position and trajectory it was observed that in all cases occurred tropopause folding with subsiding air west of the folding and inside it while east of it there was ascending air and values of relative humidity between 10 and 20% coinciding with the dynamic tropopause. The stratospheric dry air with high values of potential vorticity is intruded through the tropopause anomalies into the high and mid-troposphere inducing the cyclogenesis at the surface.

Further all six cases presented upper level confluence of the subtropical and polar jet streams over South America and near the east coast under the influence of a trough in the equatorward side of the subtropical jet stream and a ridge in the polar side of the polar jet

stream. In that confluence a jet streak occurs with diffluence downstream. In the exit region of the jet streak the cyclogenesis takes place in the surface.

It was observed that in all the cases the cyclogenesis intensity was associated with the jet streams perturbations of baroclinic origin.

Also the local where the cyclogenesis begins showed influence in the intensity, reason why the analysis by composite fields was not performed here. When it begins in higher latitudes the trajectory tends to be more zonal and the intensity to be smaller.

Another interesting confirmation indicated from all six cases selected and analyzed was that the explosive cyclones develop following the Shapiro & Keyser (1990) cyclone conceptual model after which the cold front move perpendicular to the warm front because of the stratospheric air intrusion near the cyclone center, creating a katafront pattern in which the warm air that should ascend over the frontal ramp (warm conveyor belt) is pushed above by the dry air intrusion and have to return. In the traditional Bjerknes & Solberg (1922) the cold front turns like a clock pointer till it reaches cold air ahead the warm front raising the warm air in a process called occlusion. In the conceptual model of Shapiro & Keyser (1990) when the dry air intrusion pushes the warm air making it return above part of the warm air remains trapped below the air of the intrusion in a process called seclusion ascending slowly through the cold air later. This characteristic was confirmed by the study of all eleven strong cases occurred between 2012 and 2016 (V.D. Avila et al., unpublished data).

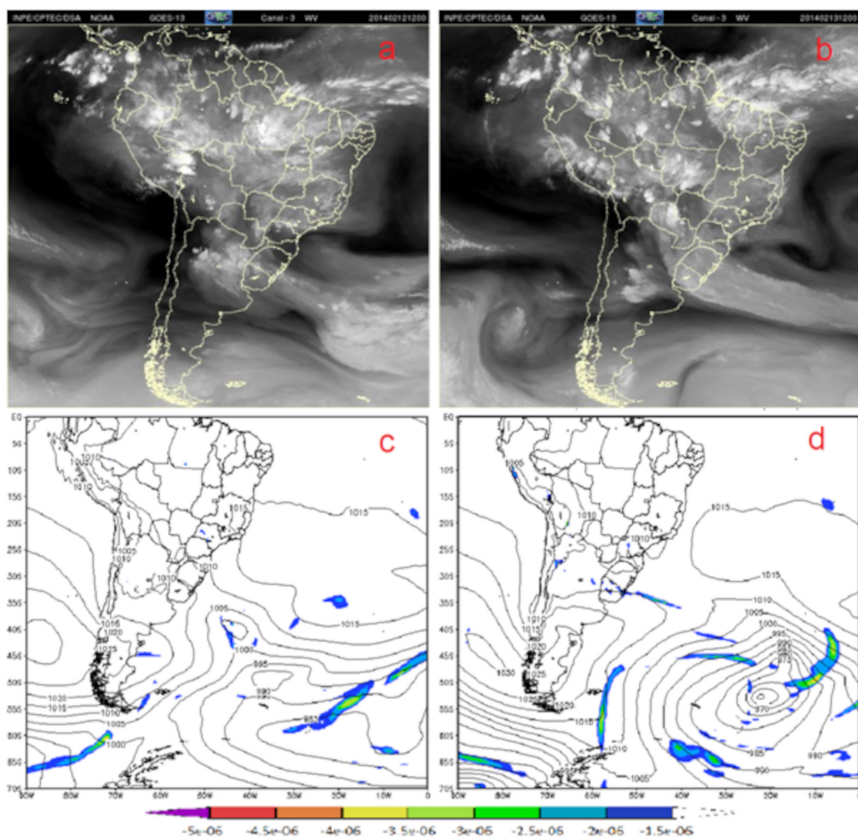


Figure 7. Satellite GOES-13 water vapor channel imagery (above) and EPV in the 500 hPa level (color shaded) with MSLP contours (below) respectively in the beginning of the explosive development of the cyclone (a and c – 02/12/2014, 12Z) and at the end of this cycle (b and d – 02/13/2014, 12Z).

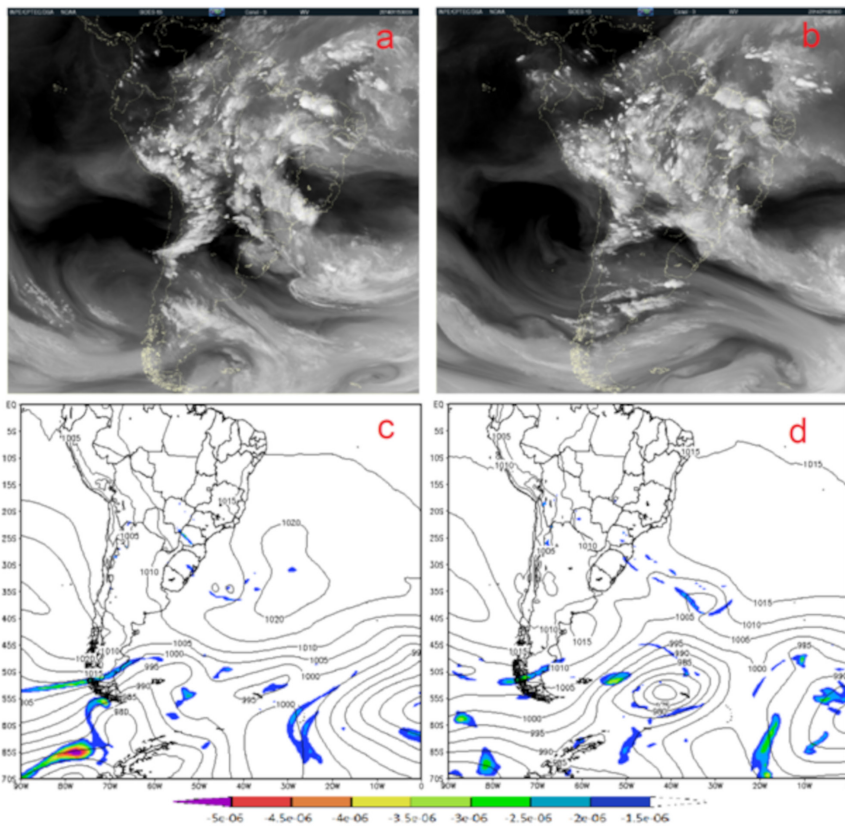


Figure 8. Satellite GOES-13 water vapor channel imagery (above) and EPV in the 500 hPa level (color shaded) with MSLP contours (below) respectively in the beginning of the explosive development of the cyclone (a and c – 01/15/2014, 00Z) and at the end of this cycle (b and d – 01/16/2014, 00Z).

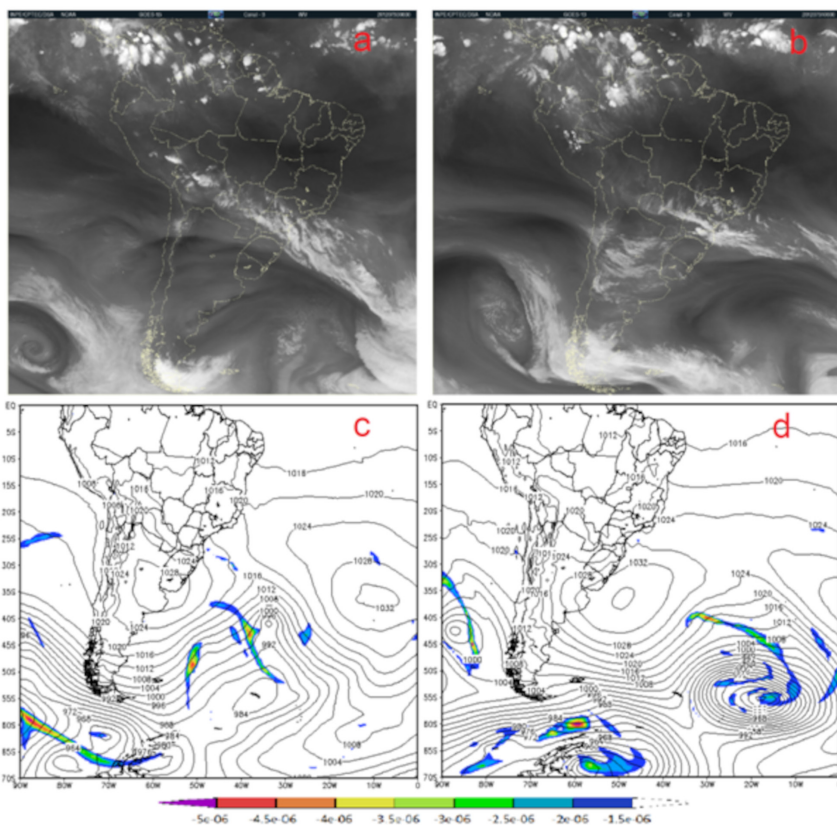


Figure 9. Satellite GOES-13 water vapor channel imagery (above) and EPV in the 500 hPa level (color shaded) with MSLP contours (below) respectively in the beginning of the explosive development of the cyclone (a and c – 07/30/2012, 06Z) and at the end of this cycle (b and d – 07/31/2012, 06Z).

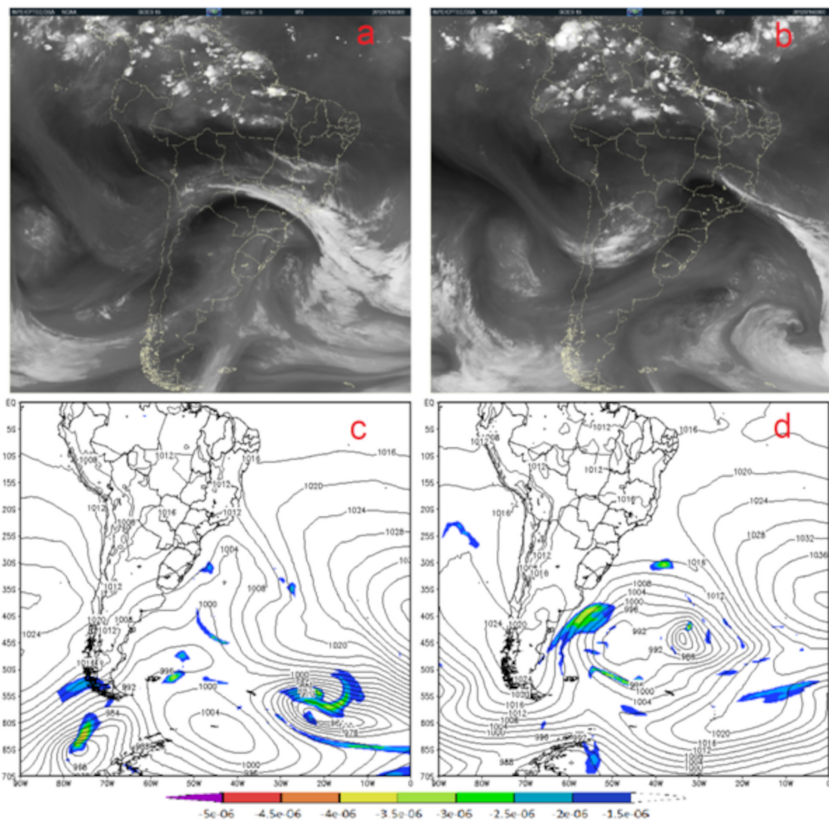


Figure 10. Satellite GOES-13 water vapor channel imagery (above) and EPV in the 500 hPa level (color shaded) with MSLP contours (below) respectively in the beginning of the explosive development of the cyclone (a and c – 07/13/2012, 00Z) and at the end of this cycle (b and d – 07/14/2012, 00Z).

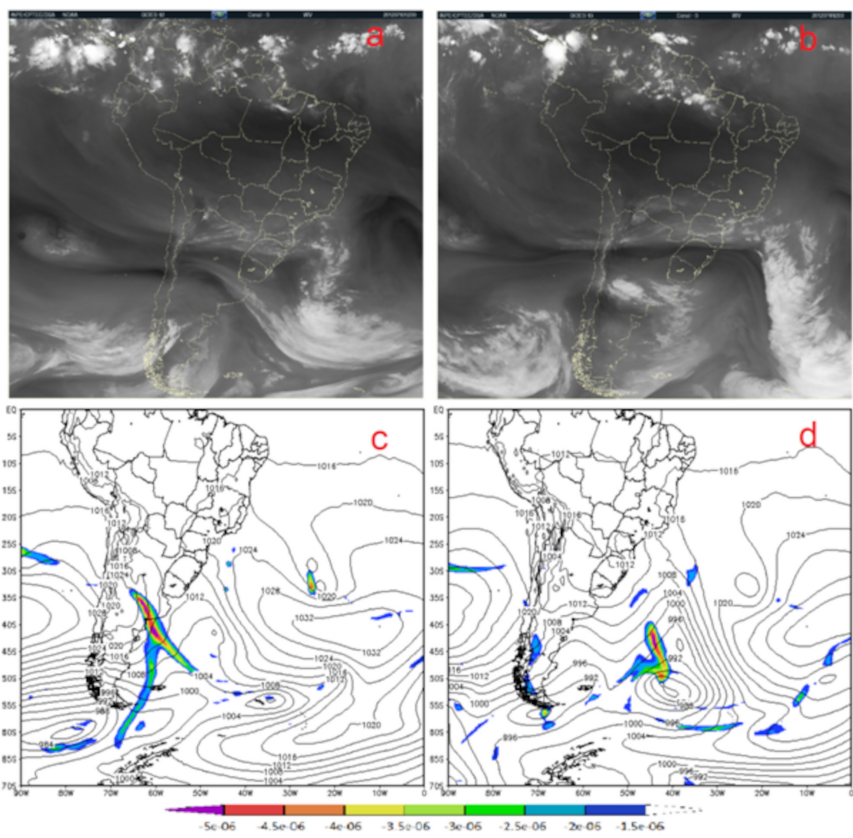


Figure 11. Satellite GOES-13 water vapor channel imagery (above) and EPV in the 500 hPa level (color shaded) with MSLP contours (below) respectively in the beginning of the explosive development of the cyclone (a and c - 07/10/2012, 12Z) and at the end of this cycle (b and d - 07/11/2012, 12Z).

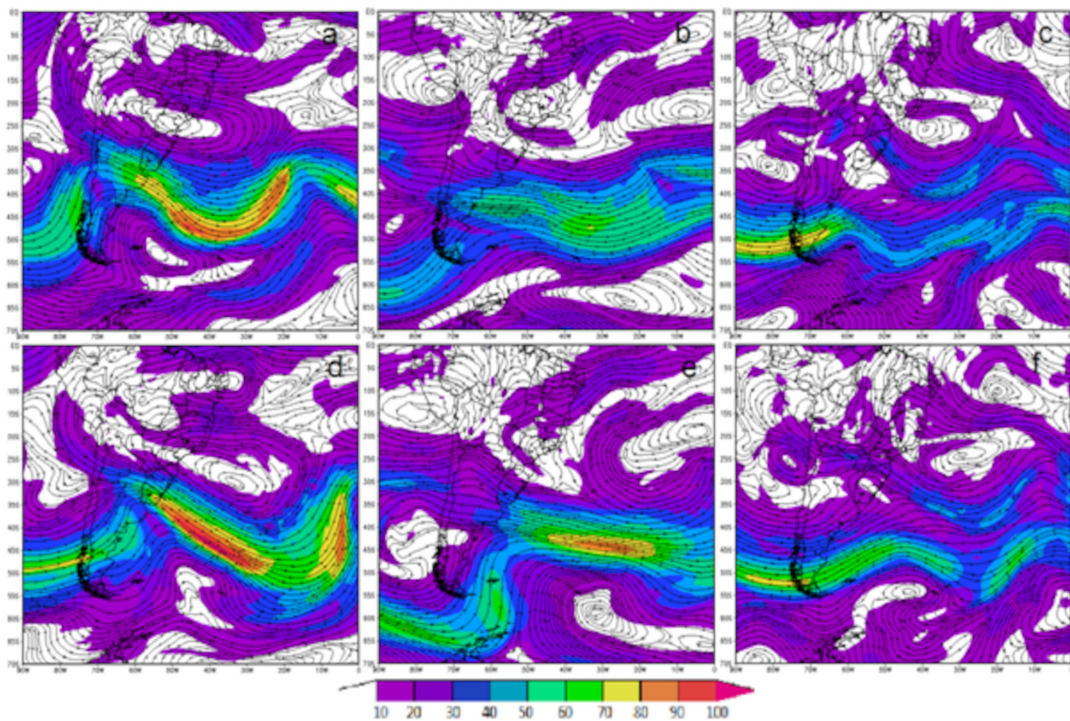


Figure 12. Wind magnitude in ms^{-1} (shaded) and streamlines at 250 hPa (contours) in the beginning of the explosive cycle (a- 01/03/2014, 00Z; b- 02/12/2014, 12Z; c- 01/15/2014, 00Z) and in the end of the cycle (d- 01/04/2014, 00Z; e- 02/13/2014, 12Z; f- 01/16/2014, 00Z).

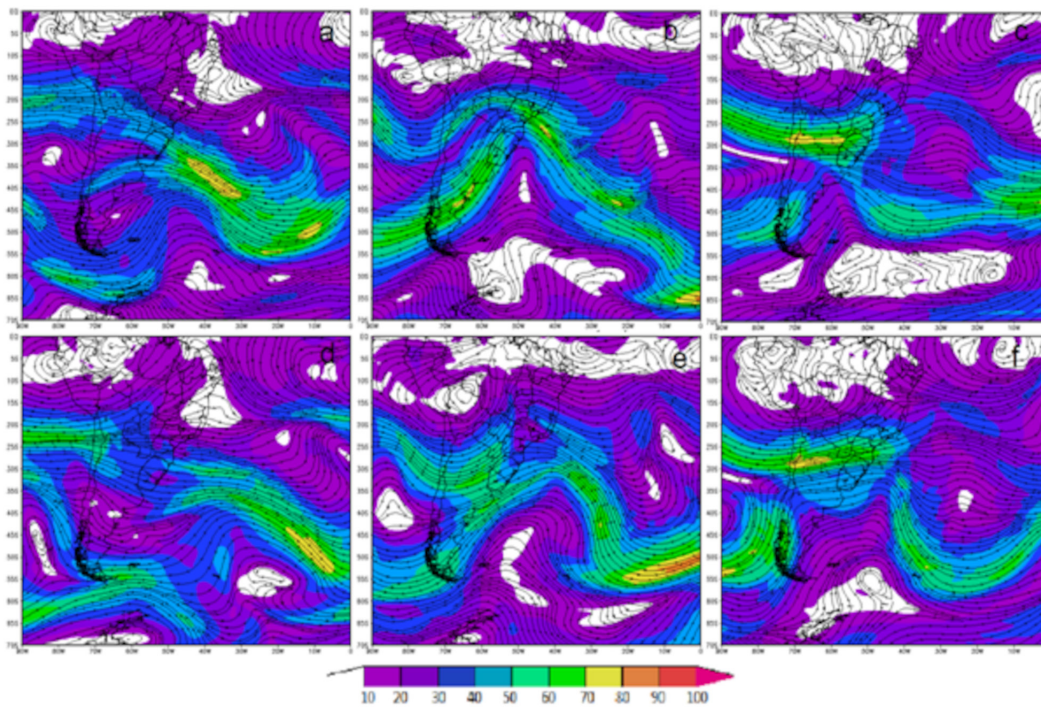


Figure 13. Wind magnitude in ms^{-1} (shaded) and streamlines at 250 hPa (contours) in the beginning of the explosive cycle (a- 07/30/2012, 06Z; b- 07/13/2012, 00Z; c- 07/10/2012, 12Z) and in the end of the cycle (d- 07/31/2012, 06Z; e- 07/14/2012, 00Z; f- 07/11/2012, 12Z).

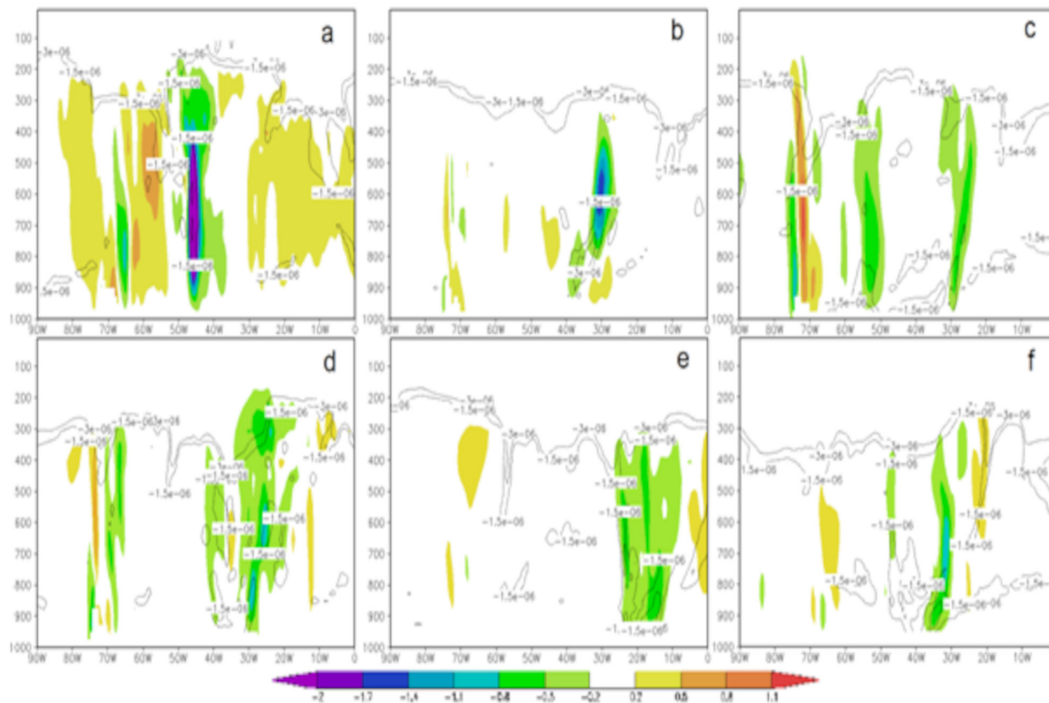


Figure 14. Vertical zonal sections of $\text{EPV} \geq 1.5 \text{PVU}$ contours (in module) and omega in color shading at the latitudes where the cyclones were localized at the beginning of the explosive development: (a- 01/03/2014, 00Z, 40°S; b- 02/12/2014, 12Z, 50°S; c- 01/15/2014, 00Z, 51°S), and at the end of the explosive cycle: (d- 01/04/2014, 00Z, 50°S; e- 02/13/2014, 12Z, 53°S; f- 01/16/2014, 00Z, 55°S).

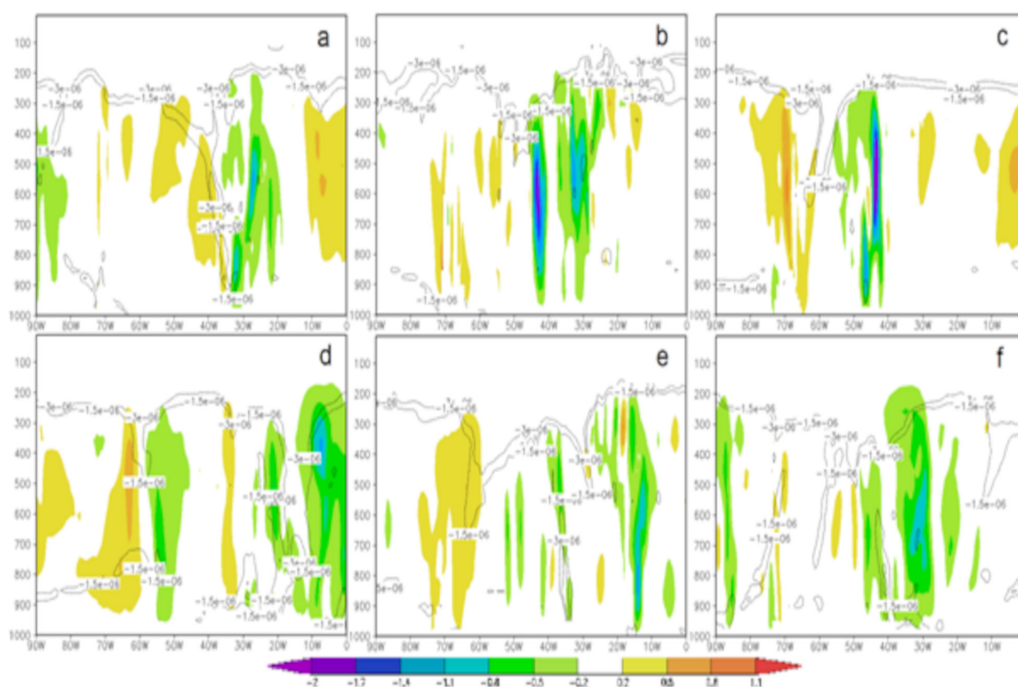


Figure 15. Vertical zonal sections of $EPV \geq 1.5 PVU$ contours (in module) and omega in color shading at the latitudes where the cyclones were localized at the beginning of the explosive development: (a- 07/30/2012, 06Z, 40°S; b- 07/13/2012, 00Z, 33°S; c- 07/10/2012, 12Z, 42°S), and at the end of the explosive cycle: (d- 07/31/2012, 06Z, 56°S; e- 07/14/2012, 00Z, 44°S; f- 07/11/2012, 12Z, 53°S).

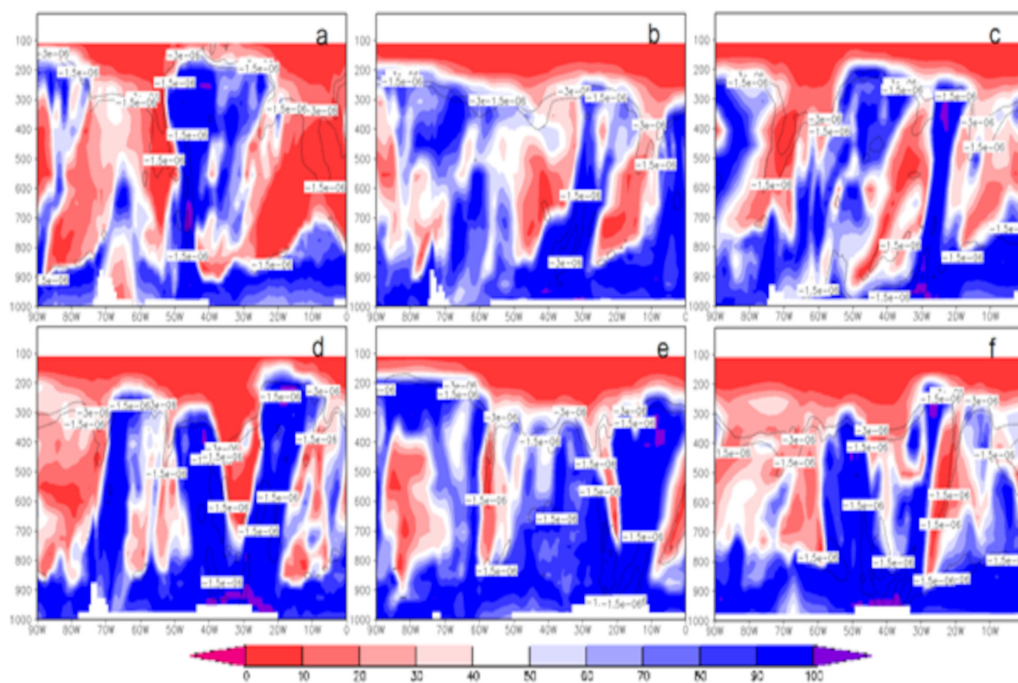


Figure 16. Vertical zonal sections of $EPV \geq 1.5 PVU$ contours (in module) and relative humidity in color shading at the latitudes where the cyclones were localized at the beginning of the explosive development: (a- 01/03/2014, 00Z, 40°S; b- 02/12/2014, 12Z, 50°S; c- 01/15/2014, 00Z, 51°S), and at the end of the explosive cycle: (d- 01/04/2014, 00Z, 50°S; e- 02/13/2014, 12Z, 53°S; f- 01/16/2014, 00Z, 55°S).

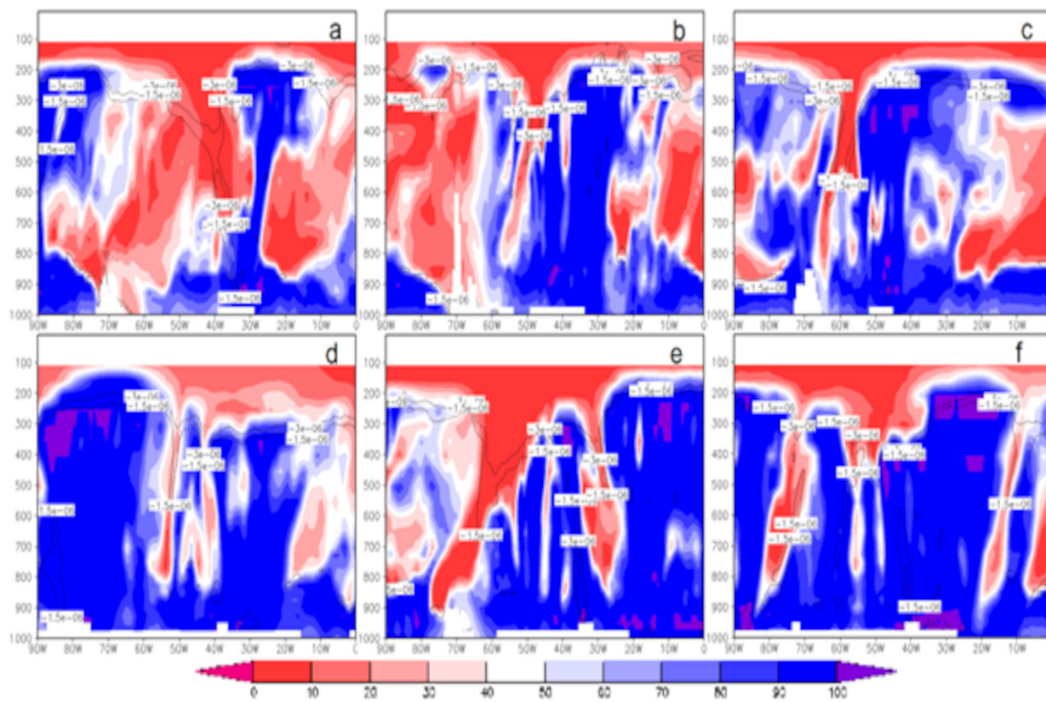


Figure 17. Vertical zonal sections of $EPV \geq 1.5$ PVU contours (in module) and relative humidity in color shading at the latitudes where the cyclones were localized at the beginning of the explosive development: (a- 07/30/2012, 06Z, 40°S; b- 07/13/2012, 00Z, 33°S; c- 07/10/2012, 12Z, 42°S), and at the end of the explosive cycle: (d- 07/31/2012, 06Z, 56°S; e- 07/14/2012, 00Z, 44°S; f- 07/11/2012, 12Z, 53°S).

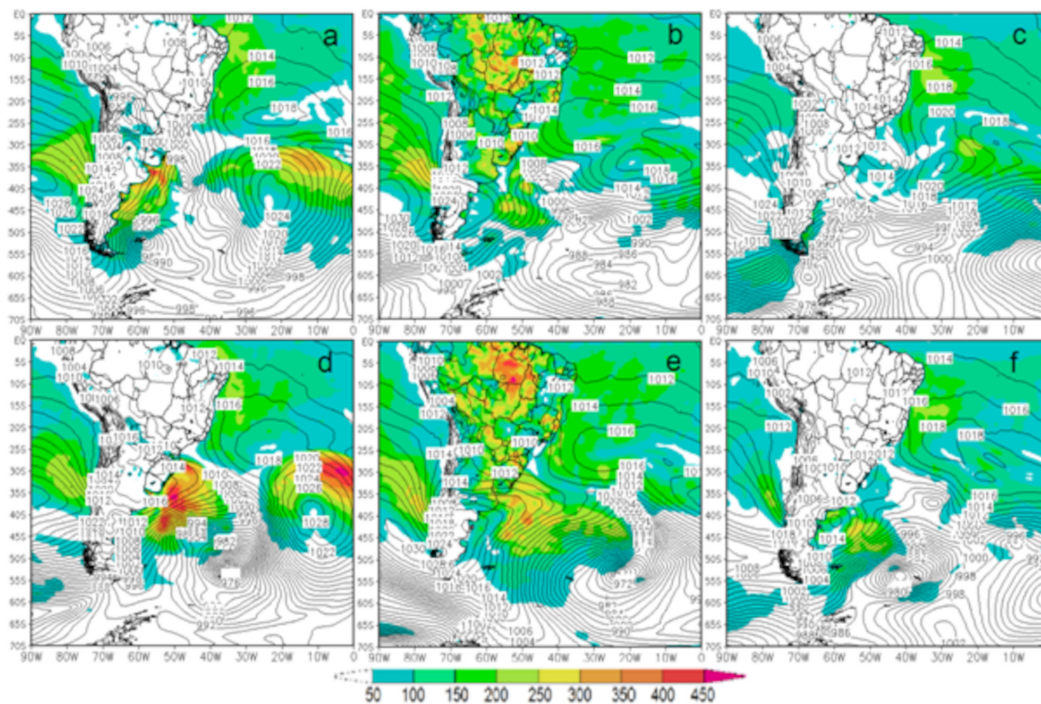


Figure 18. MSLP contours (black) and Latent Heat Flux (color shading). Initial positions: (a- 01/03/2014, 00Z; b- 02/12/2014, 12Z; c- 01/15/2014, 00Z), and final positions: (d- 01/04/2014, 00Z; e- 02/13/2014, 12Z; f- 01/16/2014, 00Z).

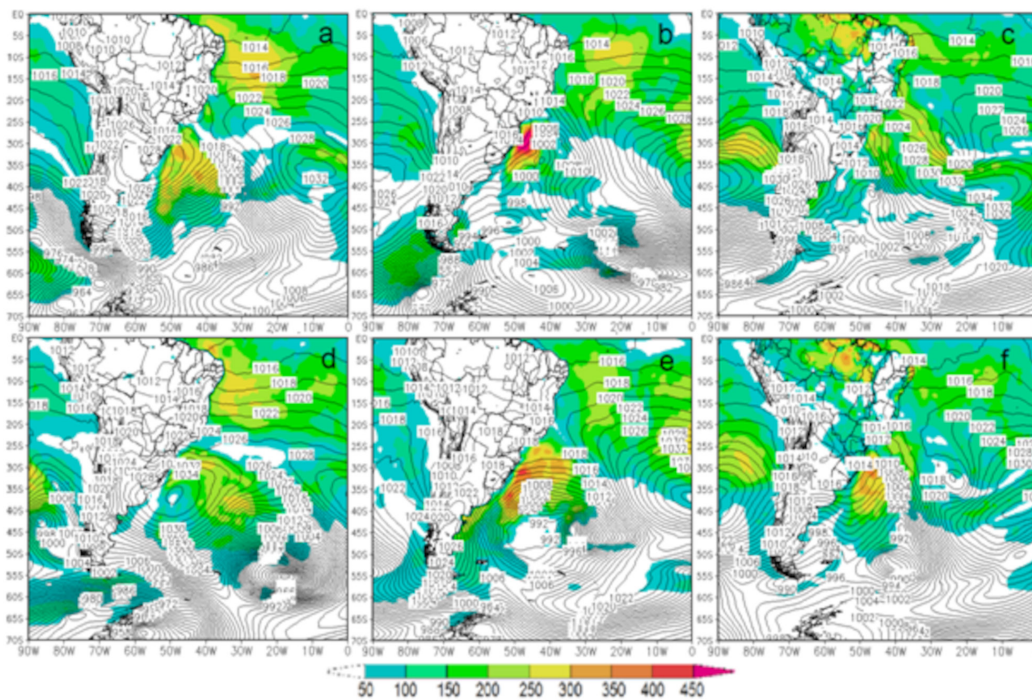


Figure 19. MSLP contours (black) and Latent Heat Flux (color shading). Initial positions: (a- 07/30/2012, 06Z, 40°S; b- 07/13/2012, 00Z, 33°S; c- 07/10/2012, 12Z, 42°S), and at the end of the explosive cycle: (d- 07/31/2012, 06Z, 56°S; e- 07/14/2012, 00Z, 44°S; f- 07/11/2012, 12Z, 53°S).

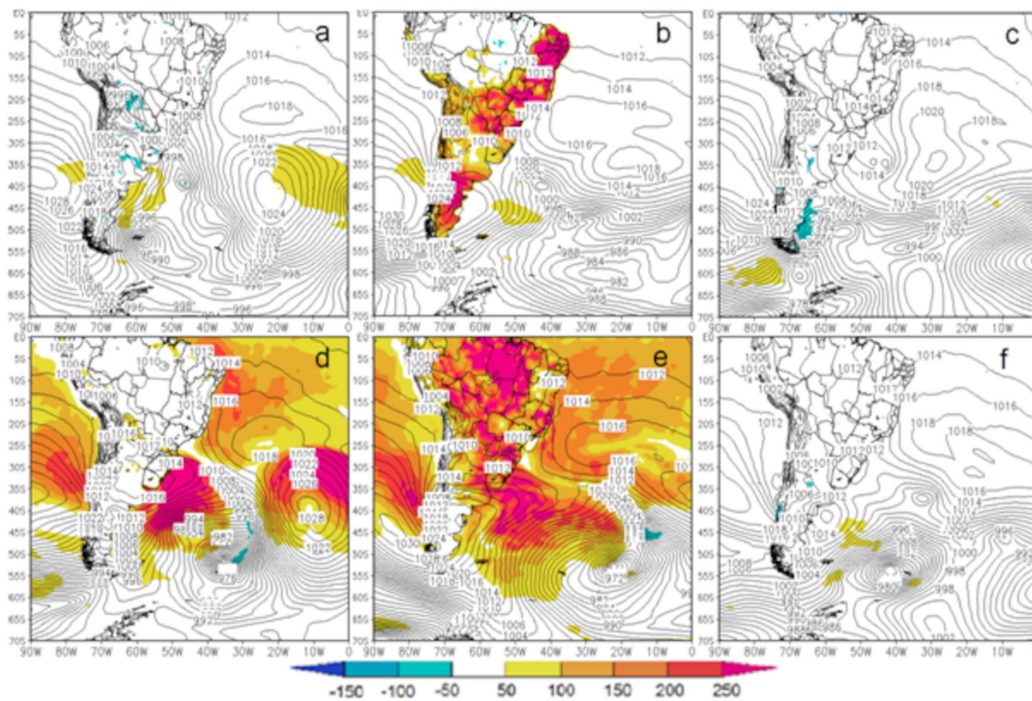


Figure 20. MSLP contours (black) and Sensible Heat Flux due to turbulence (color shading). Initial positions: (a- 01/03/2014, 00Z; b- 02/12/2014, 12Z; c- 01/15/2014), 00Z), and final positions: (d- 01/04/2014, 00Z; e- 02/13/2014, 12Z; f- 01/16/2014, 00Z).

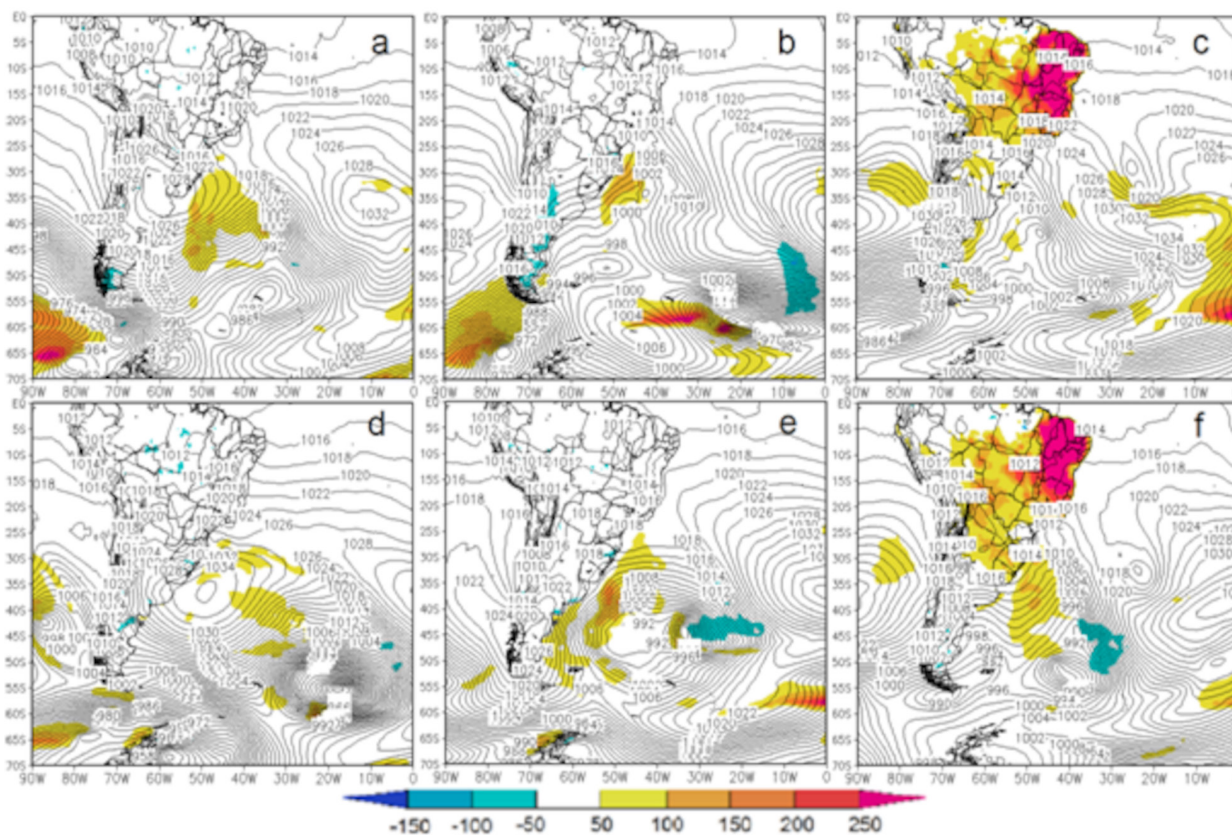


Figure 21. MSLP contours (black) and Sensible Heat Flux due to turbulence (color shading). Initial positions: (a- 07/30/2012, 06Z, 40°S; b- 07/13/2012, 00Z, 33°S; c- 07/10/2012, 12Z, 42°S), and at the end of the explosive cycle: (d- 07/31/2012, 06Z, 56°S; e- 07/14/2012, 00Z, 44°S; f- 07/11/2012, 12Z, 53°S).

REFERENCES

- ALLEN JT, PEZZA AB & BLACK MT. 2010. Explosive cyclogenesis: A global climatology comparing multiple reanalysis. *J Climate* 23(24): 6468-6484.
- AVILA VD, NUNES AB & ALVES RCM. 2016. Análise de um caso de ciclogênese explosiva ocorrido em 03/01/2014 no sul do oceano Atlântico. *Rev Bras Geogr Fis* 9(4). <http://dx.doi.org/10.5935/1984-2295.20160074>.
- BECHIS H, GODOY AA, POSSIA NE & CAMPETELLA CM. 2018. Analisis de la presión de la tropopausa dinámica en bajas segregadas del sur de Sudamérica. *Meteorológica* 43(1): 25-40.
- BITENCOURT DP, FUENTES MV & CARDOSO CS. 2013. Climatologia de Ciclones Explosivos Para a Área Ciclogênica da América do Sul. *Rev Bras Meteorol* 28(1): 43-56.
- BJERKNES J. 1919. On the structure of moving cyclones. *Geophys Publ* 1(2): 1-8.
- BJERKNES J & SOLBERG H. 1922. Life cycle of cyclones and the polar front theory of atmospheric circulation. *Geophys Publ* 3: 3-18.
- BLACK MT & PEZZA AB. 2013. A universal, broad-environment energy conversion signature of explosive cyclones. *Geophys Res Lett* 40: 452-457.
- BLUESTEIN HB. 1993. *Synoptic-Dynamic Meteorology in Midlatitudes. Volume II: Observations and theory of weather systems.* Oxf Univ Press. Oxford, 594 p.
- GAN MA & RAO VB. 1991. Surface cyclogenesis over South America. *Mon Wea Rev* 119(5): 1293-1302.
- GELARO R ET AL. 2017. The modern-era retrospective analysis for research and applications, version 2 (MERRA-2). *J Climate* 14: 5419-5454. doi:10.1175/JCLI-D-16-0758.1.
- GIORDANI H & CANIAUX G. 2001. Sensitivity of cyclogenesis to sea surface temperature in the northwestern Atlantic. *Mon Wea Rev* 129(6): 1273-1295.

- HODGES KI, LEE RW & BENGTTSSON L. 2011. A comparison of extratropical cyclones in recent reanalyses ERA-Interim, NASA MERRA, NCEP CFSR, and JRA-25. *J Climate* 24: 4888-4906.
- HOSKINS BJ & HODGES KI. 2005. A New Perspective on Southern Hemisphere Storm Tracks. *J Climate* 18: 4108-4129.
- HOSKINS BJ, MCINTYRE ME & ROBERTSON AW. 1985. On the use and significance of isentropic potential vorticity maps. *Q J R Meteorol Soc* 111: 877-946.
- IWABE CMN & ROCHA RP. 2009. An event of stratospheric air intrusion and its associated secondary surface cyclogenesis over the South Atlantic Ocean. *J Geophys Res* 114: D09101. doi:10.1029/2008JD011119.
- LIM EP & SIMMONDS I. 2002. Explosive cyclone development in the Southern Hemisphere and a comparison with Northern Hemisphere Events. *Mon Wea Rev* 130(9): 2188-2209.
- MENDES D, SOUZA EP, MARENGO JA & MENDES MCD. 2010. Climatology of extratropical cyclones over the South American-southern oceans sector. *Theor Appl Climatol* 100(3-4): 239-250.
- MURRAY RJ & SIMMONDS I. 1991. A numerical scheme for tracking cyclone centres from digital data. Part I: Development and operation of the scheme. *Aust Meteor Mag* 39: 155-166.
- NAUD CM, BOOTH JF & DEL GENIO AD. 2014. Evaluation of ERA-Interim and MERRA cloudiness in the Southern Ocean. *J Climate* 27: 2109-2124.
- NECCO G. 1982. Comportamiento de vortices ciclonicos en el area Sudamericana durante el FGGE : Ciclogenesis. *Meteorológica* 13(1-2): 7-19.
- NUNES AB & AVILA VD. 2017. Dynamic Tropopause Analysis: Case Study in South America. *Anu Inst Geoc UFRJ* 40: 83-92. http://dx.doi.org/10.11137/2017_1_83_92.
- PALMEN E & NEWTON CM. 1969. *Atmospheric Circulation Systems*. Acad Press, 603 p.
- PETTERSSSEN S. 1956. *Motion and Motion Systems*, New York: McGraw Hill 1: 428 p.
- PEZZI LP, SOUZA RB, FARIAS PC, ACEVEDO O & MILLER AJ. 2016. Airsea interaction at the Southern Brazilian Continental Shelf: In situ observations. *J Geophys Res Oceans* 121(9): 6671-6695. doi:10.1002/2016JC011774.
- PINTO JRD & ROCHA RP. 2011. The energy cycle and structural evolution of cyclones over southeastern South America in three case studies. *J Geophys Res* 116: D14112. doi:10.1029/2011JD016217.
- PIVA E, GAN MA & MOSCATI MCL. 2011. The role of latent and sensible heat fluxes in an explosive cyclogenesis over South America. *J Met Soc Japan* 89(6): 1-27. doi:10.2151/jmsj.2011-604.
- QUADRO MFL, SILVA DIAS MA, HERDIES DL & GONÇALVES LGG. 2012. Análise climatológica da precipitação e do transporte de umidade na região da ZCAS através da nova geração de reanálises. *Rev Bras Meteorol* 27: 152-162.
- REBOITA MS, GAN MA, DA ROCHA RP & AMBRIZZI T. 2010. Regimes de Precipitação na América do Sul: Uma Revisão Bibliográfica. *Rev Bras Meteorol* 25(2): 185-204.
- REBOITA MS, ROCHA RP & AMBRIZZI T. 2005. Climatologia de Ciclones sobre o Atlântico Sul Utilizando Métodos Objetivos na Detecção destes Sistemas. In: IX CONGRESMET, CONG. ARGENTINO MET. Buenos Aires, AR, Outubro 3-7.
- REED RJ. 1955. A study of a characteristic type of upper-level frontogenesis. *J Meteor* 12: 226-237.
- SANDERS F. 1986. Explosive cyclogenesis in the West-Central North Atlantic Ocean, 1981-84. Part I: Composite structure and mean behavior. *Mon Wea Rev* 114(10): 1781-1794.
- SANDERS F & GYAKUM JR. 1980. Synoptic-dynamic climatology of the "Bomb". *Mon Wea Rev* 108(10): 1589-1606.
- SANTURETTE P & GEORGIEV CG. 2005. *Weather analysis and forecasting: Applying satellite water vapor imagery and potential vorticity analysis*. Acad Press, Amsterdam, 179 p.
- SATYAMURTY P, FERREIRA CC & GAN MA. 1990. Cyclonic vortices over South America. *Tellus A* 42A(1): 194-201.
- SCHUBERT WH, RUPRECHT E, HERTENSTEIN R, FERREIRA RN, TAFT R, ROZOFF C, CIESIELSKI P & KUO H-C. 2004. English translations of twenty-one of Ertel's papers on geophysical fluid dynamics. *Meteor Zeit* 13(6): 527-576. doi:10.1127/0941-2948/2004/0013-0527.
- SHAPIRO MA & KEYSER D. 1990. Fronts, jet streams and the tropopause. *Extratropical Cyclones, The Erik Palmén Memorial Volume*, Newton CW and Holopainen EO (Eds), Am Meteor Soc, p. 167-191.
- SIMMONDS I & KEAY K. 2000. Mean southern hemisphere extratropical cyclone behavior in the 40-year NCEP-NCAR reanalysis. *J Climate* 13(5): 873-885.
- SINCLAIR MR. 1995. A climatology of cyclogenesis for the Southern Hemisphere. *Mon Wea Rev* 123(6): 1601-1619.
- SUTCLIFFE RC. 1947. A contribution to the problem of development. *Q J R Meteorol Soc* v 73: 370-383. doi:10.1002/qj.49707331710.

TALJAARD JJ. 1967. Development, distribution and movement of cyclones and anticyclones in the Southern Hemisphere during the IGY. *J Appl Meteor* 6(6): 973-987.

UCCELLINI LW, KEYSER D, BRILL KF & WASH CH. 1985. The President's Day Cyclone of 18-19 February 1979: Influence of upstream trough amplification and associated tropopause folding on rapid cyclogenesis. *Mon Wea Rev* 113: 962-988.

WANG C-C & ROGERS JC. 2001. A composite study of explosive cyclogenesis in different sectors of the North Atlantic. Part I: Cyclone structure and evolution. *Mon Wea Rev* 129: 1481-1499.

How to cite

AVILA VD, NUNES AB & ALVES RCM. 2021. Comparing explosive cyclogenesis cases of different intensities occurred in Southern Atlantic. *An Acad Bras Cienc* 93: e20190157. DOI 10.1590/0001-3765202120190157.

*Manuscript received on May 3, 2019;
accepted for publication on April 28, 2020*

VILSON D. DE AVILA¹

<https://orcid.org/0000-0001-5998-1155>

ANDRÉ B. NUNES²

<https://orcid.org/0000-0002-4881-5810>

RITA DE CÁSSIA M. ALVES¹

<https://orcid.org/0000-0001-7804-8141>

¹Programa de Pós-Graduação em Sensoriamento Remoto, Universidade Federal do Rio Grande do Sul, Av. Bento Gonçalves, 9500, Campus Vale, 91501-970 Porto Alegre, RS, Brazil

²Programa de Pós-Graduação em Meteorologia, Universidade Federal de Pelotas, Av. Ildefonso Simões Lopes, 2751, 96060-290 Pelotas, RS, Brazil

Correspondence to: **Vilson Dias de Avila**

E-mail: vilson.ufrgs@gmail.com

Author contributions

VD Avila was the main author of the project idea, responsible for the elaboration and execution of the methodology, bibliographic survey, generation and analysis of the results as well as preparing and formatting the text. AB Nunes collaborated in obtaining numerical data, scripts execution, illustrations generation and in the analysis of some results. RCM Alves collaborated in the general review, specially in the bibliographic review and results with emphasis in satellite image interpretation.

